Effect of different curing regimes on the mechanical and durability properties of alkali-activated products containing slag, silica fume, and limestone powder

Ebrahim Ghiasvand[1*], Mohammad Swete[2], Seyed Amirali Razavi[2]
[1] Assistant Professor, Faculty of Engineering, Bu Ali Sina University, Hamedan, Iran.
[2]Faculty of Engineering, Buali Sina University, Hamedan, Iran.

* e.ghiasvand@basu.ac.ir

Abstract:
Portland cement production is a major source of greenhouse gas emissions, and while the integration of supplementary cementitious materials (SCMs) and alkali-activated materials (AAMs) offers a sustainable pathway to reduce environmental impacts and enhance durability, the effectiveness of these systems is critically governed by curing regimes that determine strength development and long-term performance. In this study investigates the influence of curing regimes on the performance of alkali-activated concretes incorporating ground granulated blast-furnace slag (GGBS) with silica fume (SF) and limestone powder (LP). Concretes were activated using sodium hydroxide (8M) and sodium silicate (water glass) with a silicate modulus of 2.07, and subjected to five curing conditions. Mechanical and durability properties were assessed through volumetric water absorption, rapid chloride permeability test (RCPT), and rapid chloride migration test (RCMT) at 90 days, and compressive strength at 28 and 90 days. Results showed that the specimen containing 85% GGBS and 15% LP exhibited favorable strength and durability under water curing, indicating its suitability for practical applications. In contrast, steam curing caused a sustained reduction in compressive strength, while permeability performance showed no significant improvement. These findings highlight the importance of curing conditions in developing durable, environmentally sustainable geopolymer concretes for broader construction use.

Keywords: Alkali-activated materials, Geopolymer concrete, Curing regimes, Concrete durability, Compressive strength

1- Introduction

Environmental sustainability and the development of eco-friendly construction materials have attracted considerable attention from both researchers and policymakers. The growing adoption of such materials is largely driven by the availability of raw ingredients, cost-effective production, favorable mechanical properties, and enhanced durability [1]. Concrete remains the most widely utilized construction material worldwide, with its production expected to continue rising. However, Portland cement, a key component in concrete, is associated with substantial greenhouse gas emissions during manufacturing, and Portland cement-based products frequently exhibit inadequate long-term durability [2].

Concrete durability is defined as its capacity to withstand weathering, chemical attack, abrasion, freeze–thaw cycles, and other forms of deterioration [3]. The ingress of water and deleterious ions, particularly chlorides, through pore networks can initiate reinforcement corrosion, thereby impairing performance and reducing service life [4, 5]. The permeability of hardened concrete is affected by the size, distribution, and continuity of pores and holes in it. Diffusion of aggressive ions inside the concrete, through existing holes

that occur in the cement matrix and the interfacial transition zone (ITZ) [6, 7].

Some studies have demonstrated that replacing ordinary Portland cement (OPC) with supplementary cementitious materials (SCMs) can refine the pore structure, reduce permeability, and enhance durability [8-16]. Among these alternatives, alkali-activated materials (AAMs) have gained significant attention due to their growing application and promising performance characteristics.

Alkali-activated materials (AAMs), also known as geopolymers, are produced by combining aluminosilicate-rich base materials with alkaline activators, resulting in the dissolution and reorganization of aluminum and silicon ions into a geopolymer matrix [17, 18]. Compared to conventional Portland cement concrete, AAMs exhibit faster setting, adequate compressive strength, reduced water absorption, and enhanced durability, making them a promising sustainable alternative [19-22].

Hydration and geopolymerization represent distinct reaction mechanisms in cementitious systems. Hydration occurs under water-rich, ambient curing conditions through the interaction of clinker phases (C_3S, C_2S, C_3A, C_4AF) with water, producing calcium silicate hydrate (C-S-H), calcium hydroxide, and ettringite, alongside porosity. While hydration enables rapid strength gain, it is exothermic and may cause thermal cracking, and its products remain vulnerable to chemical degradation under sulfate or chloride exposure, contributing to a high carbon footprint [23-25].

In contrast, geopolymerization involves the dissolution of aluminosilicate precursors (e.g., fly ash, slag, metakaolin) in alkaline activators such as NaOH or sodium silicate, followed by polycondensation into sodium aluminosilicate hydrate (N-A-S-H) or calcium aluminosilicate hydrate (C-A-S-H) gels. Elevated curing temperatures accelerate geopolymerization kinetics and improve mechanical performance, making it a promising alternative to conventional hydration-based systems [26-30].

Given the pronounced influence of curing conditions on the performance of geopolymer concrete, it is essential to examine how different curing regimes affect its compressive strength and permeability [31-37]. Runci and Serdar [35], examined the influence of curing duration on chloride ion diffusion resistance in alkali-activated slag concrete (AASC), reporting that significant resistance to chloride penetration was achieved only after seven days of curing.

Nodehi et al. [32] provided a comprehensive review of recent advances in optimizing the mechanical performance, durability, and microstructural characteristics of alkali-activated materials (AAMs) under various curing regimes. Their findings indicate that sealing and microwave curing are the most effective approaches for both single and binary binder systems, whereas water curing and prolonged steam curing are unsuitable due to activator dilution and increased free water in concrete pores.

Jittin et al. [34] investigated three curing regimes (lime water, ambient, and controlled heat at 25 °C) to assess their impact on the strength and durability of alkali-activated concrete (AAC). Their results revealed that specimens cured under ambient conditions exhibited higher compressive strength and improved oxygen permeability indices compared to steam-cured specimens, independent of activator type, molarity, or curing duration. Additionally, specimens cured in lime water demonstrated lower water absorption relative to other regimes.

Athira et al. [31] explored the combined effects of curing regimes and base material substitution, including ground granulated blast-furnace slag (GGBS) and fly ash, on AAC properties. Their study showed that ambient curing yielded higher compressive strength in GGBS-based specimens compared to fly ash-based specimens. Fly ash systems required elevated temperatures to initiate reactions, with high-temperature curing enhancing early strength in both systems. Furthermore, blends of GGBS and fly

ash exhibited superior strength development, as GGBS contributed to early-age strength while fly ash enhanced later-age performance.

Noushini and Castel [38] investigated steam curing effects on the interfacial transition zone (ITZ) of low-calcium fly ash-based geopolymer concrete. They reported that curing at 75 °C for 18–24 hours reduced permeable voids and water absorption. Similarly, Balcikanli and Ozbay [39] evaluated thermal conductivity and chloride/oxygen permeability in AASC, identifying an optimal curing regime of 50 °C for 8 hours with a sodium concentration of 5.5%, which minimized thermal conductivity and ion penetration while maximizing compressive strength.

Although prior research has provided valuable insights into alkali-activated materials (AAMs), limited attention has been directed toward the formulation of geopolymer mixtures that are suitable for large-scale construction under conventional curing conditions. The ability to synthesize geopolymer concrete within such regimes represents a critical step toward enhancing practical applicability and enabling broader adoption of geopolymer technology in the construction industry. Nevertheless, large-scale implementation remains constrained by issues such as early-age shrinkage and reductions in mechanical and durability performance under certain curing conditions. Addressing these limitations requires curing strategies specifically tailored to the chemical composition of the mixture, a research area that remains insufficiently explored [32, 40].

This study aims to identify the optimal constituent proportions for improving the mechanical and durability performance of geopolymer concrete. To achieve this, five mixtures were designed incorporating ground granulated blast-furnace slag (GGBS) with varying weight percentages of silica fume (SF) and limestone powder (LP). The performance of these mixtures was systematically evaluated under five distinct curing regimes, including saturated lime water and steam curing, in order to determine the most suitable formulation for application in conventional structural systems.

2- Materials and methods

The control specimens were prepared using Type II Portland cement manufactured by the Hegmatan Cement Factory in Hamedan Province, with a minimum 28-day compressive strength of 240 kg/cm². Ground granulated blast furnace slag (GGBS), with an activity index of 80, was obtained as a by-product from the Isfahan Zob Ahan Company and subsequently processed by Madaen Cement Company in Isfahan. The silica fume utilized in this study was sourced from Ferrosilicon Co. in Azna County, Lorestan Province. Limestone powder was supplied from the mines of Tehran Cement Company, located in Qom Province. The physical and chemical properties of the ordinary Portland cement (OPC) and supplementary cementitious materials, including GGBS, silica fume, and limestone powder, are summarized in Table 1.

Table 1. Physical and chemical characteristics of Pozzolans (%)

Characteristic	OPC	GGBS	SF	LP
SiO_2	22.28	35.9	69.38	2.48
Al_2O_3	4.71	8.4	12.66	1.55
Fe_2O_3	2.85	0.6	2.16	0.45
CaO	65.65	37.9	2.99	51.01
MgO	1.95	8.9	1.61	2.55
Na_2O	0.155	0.3	1.513	0.196
K_2O	0.484	0.7	1.905	0.151
LOI	1.41	0.9	7.43	41.68
$CaCO_3$	-	-	-	91.1
SO_3	-	0.7	-	-
Specific weight	3.15	2.9	2.32	2.68
Blaine (cm^2/gr)	3350	4100	-	4100

Silica fume (SF) typically employed in concrete mixtures contains 85–90% silica, with high-quality grades reaching 90–95% amorphous SiO_2 [41]. In this study, however, SF with a comparatively lower SiO_2 content (~70%) was utilized to evaluate the performance of locally available materials and their suitability for concrete production under regional resource constraints.

The alkaline activator solution was prepared in liquid form with a modulus (SiO_2/Na_2O) of 2.07. An 8 M sodium hydroxide solution was obtained by dissolving 320 g of NaOH pellets in one liter of water, calculated based on the molar mass of NaOH (40 g/mol) [42]. Due to the exothermic nature of dissolution, the solution was stored for 24 hours prior to use to allow thermal stabilization.

Aggregates consisted of washed natural sand, fine sand with a maximum particle size of 12 mm, and coarse sand with a maximum particle size of 25 mm. Their physical properties are summarized in Table 2.

Table 2. Physical characteristics of aggregates

Type of material	A specific mass of saturated surface dry (t/m3)	Water absorption (%)
sand	2.65	1.73
Fine aggregate	2.66	1.32
Coarse aggregate	2.86	1.03

Due to the rapid loss of workability in alkali-activated slag cement (AASC), the use of a superplasticizer is essential to ensure proper casting and molding. In this study, a polycarboxylate-based superplasticizer supplied by a domestic manufacturer was utilized.

3- Mix preparation and curing

Five concrete mixtures were prepared and subjected to distinct curing regimes. The proportions of cementitious materials are presented in Table 3, while the detailed mixture designs are provided in Table 4. Mix designs were developed using the absolute volume method, and all specimen preparation,

sampling, and testing were carried out in the laboratory facilities of Bu Ali Sina University.

For mixing, fine and coarse aggregates were first introduced into the mixer and dry-mixed, followed by the gradual addition of water. The sodium hydroxide solution was then incorporated, after which water glass, the remaining water, and the superplasticizer were added simultaneously. Mixing was continued for 150 s to ensure homogeneity. Three specimens were prepared for each mix design at every testing age. Molding was performed in accordance with standard placement and compaction procedures, using pre-oiled molds as shown in Fig. 1. After casting, specimens were covered with plastic sheets and stored at room temperature for 24 h, then demolded and transferred to the designated curing regimes until testing. The curing regimes are summarized in Table 5.

(a) (b)

Fig. 1. a) 10x10x10 cm cube molds, b) 10x20 cm cylindrical molds

Table 3. Ratios of cement materials used in mixtures

Mixtures	Ingredients and their ratios
Mixture 1 – Control – M1	100% OPC
Mixture 2 – M2	100% GGBS
Mixture 3 – M3	92.5% GGBS + 7.5% SF
Mixture 4 – M4	85% GGBS + 15% LP
Mixture 5 – M5	75% GGBS + 7.5% SF + 17.5% LP

Table 4. Mixture design (kg/m^3)

Series	OPC	GGBS	SF	LP	Water	Sodium hydroxide	Sodium silicate	Fine	Course
M1	450	-	-	-	224.4	-	-	936.1	936.1
M2	-	344.4	-	-	83.6	103.3	103.3	884	884
M3	-	347.6	26.1	-	97.7	104.3	104.3	932	932
M4	-	305.6	-	46	72.5	92	92	870.7	870.7
M5	-	306.2	23	53.6	113.3	91.9	91.9	926.3	926.3

Table 5. Different types of curing regimes

Curing regimes	Details of humidity and temperature curing regimes
A	Cured in saturated lime water at 23°C for 7 days
B	Cured in saturated lime water at 23°C for 28 days
C	Cured in saturated lime water at 23°C for 90 days

D	Cured in 100% humidity with a temperature of 40°C for 24 hours
E	Cured in 100% humidity with a temperature of 60°C for 24 hours

Steam curing simulates the thermal and moisture conditions typical of hot, humid climates and massive concrete elements, while offering a controlled environment that ensures consistency and reproducibility. Also, steam curing provides elevated temperature and humidity to accelerate the hydration process. Recent investigations have demonstrated that this method effectively enhances early-age strength development; however, improper curing may adversely influence long-term durability [43, 44].

4- Experimental tests

4-1- Compressive strength test

The compressive strength test is among the most widely employed methods for evaluating the mechanical properties of concrete and, in certain cases, is also used as an indicator of durability. Compressive strength is typically the primary parameter considered in the design of concrete structures. It is influenced by several factors, including the water-to-cement ratio, aggregate size, specimen dimensions and geometry, curing conditions, compaction quality, loading rate, and the type and proportion of additives and constituent materials [45]. The compressive strength test of concrete at the age of 28 and 90 days was performed according to BS EN 12390-3 standard.

4-2- Rapid Chloride penetration and migration tests (RCPT and RCMT)

The Rapid Chloride Permeability Test (RCPT), standardized as ASTM C1202, quantifies the total electrical charge (in Coulombs) passed through a concrete specimen over a six-hour period to assess its chloride ion permeability, as classified in Table 6. Originally proposed by Whiting in 1981, the method was formally adopted as ASTM C1202 in 1991[46].

As illustrated in Fig. 2(a), cylindrical specimens with a diameter of 100 mm and a thickness of 50 mm were prepared by cutting cured samples from the five designated curing regimes. After 90 days, the specimens were subjected to a two-stage vacuum saturation process—initially under vacuum without water, followed by vacuum with water—to ensure complete saturation and eliminate entrapped air, thereby enhancing test accuracy. The saturated specimens were then positioned between two cells containing 3% NaCl and 0.3 mol NaOH solutions. A constant potential difference of 60 V was applied, and the total charge passed was recorded over six hours [47].

It is important to note that the presence of ions other than chloride in the pore solution can influence the measured charge. Additionally, the high voltage applied during testing may cause a temperature rise in the specimens, particularly in low-strength concretes, where temperatures can reach up to 40 °C. This thermal effect reduces electrical resistance and consequently increases the total charge passed.

The Rapid Chloride Migration Test (RCMT) follows a similar principle but incorporates dynamic voltage adjustment based on the specimen's current response. As shown in Fig. 2(b), the initial voltage is set at 60 V, and the charge passed is monitored. If the initial current is excessive, the voltage is reduced to limit heating and maintain test integrity. After 18 ± 2 hours, the specimen is split axially, and a silver nitrate solution is applied to the exposed surface. The depth of chloride penetration is determined by measuring the extent of discoloration. The chloride migration rate (CMR) is then calculated according to AASHTO TP 357-15 using Equation (1). Table 6 presents the classification of chloride ion permeability based on

both charge passed and CMR values.

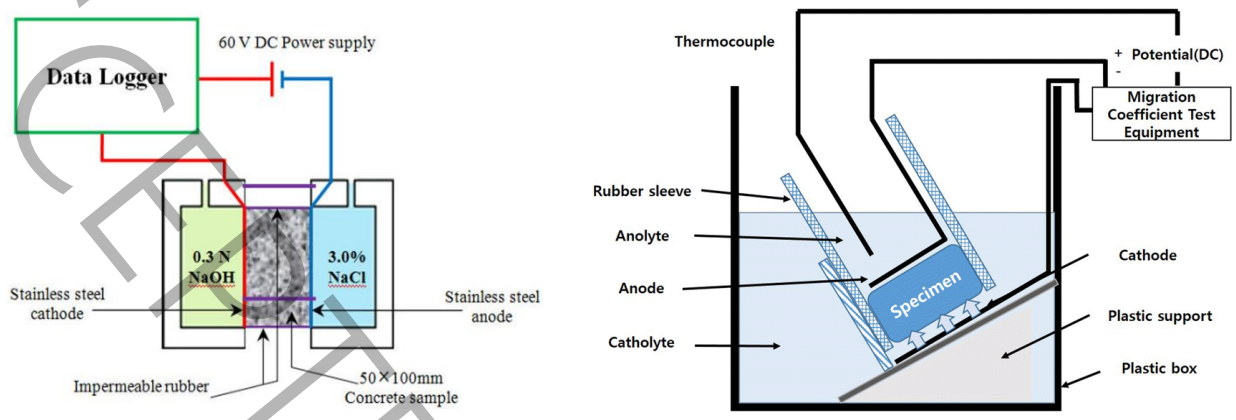

Fig. 2. a) Schematic RCP test setup, b) Schematic RCM test setup [48]

$$CMR = \frac{h}{V \times t} \tag{1}$$

where

CMR = Chloride ion migration rate (mm/V.hr)

h = the average depth of penetration (mm)

V = the applied voltage

t = the duration of the test in hours.

Table 6. Chloride ion permeability based on the results of experiments RCPT (ASTM C1202) RCMT (AASHTO TP 357-15)

Chloride permeability in concrete	CMR (mm/V.hr)	Charge passed (coulombs)
High	-	More than 4000
Moderate	0.034 > CMR > 0.024	2000-4000
Low	0.024 > CMR > 0.012	1000-2000
Very low	Less than 0.012	100-1000
Negligible	-	Less than 100

4-3- Water absorption

Volumetric water absorption is a representative indicator of concrete durability and was evaluated in accordance with BS 1881. While the standard specifies the use of 75 mm diameter cores extracted from 150 mm concrete cubes, this study employed 100 mm cube specimens without coring due to the unavailability of 300 × 150 mm cylindrical molds and time constraints during specimen preparation. Following the procedures outlined in BS 1881, the specimens are cured in different regimes until the time of testing, and after drying completely in an oven with a temperature of 110°C, they are immersed in water for 24 hours. After leaving the water, the water absorption percentage of the specimen is calculated

according to Eq. (2) by dividing the mass of the saturated surface dry specimen by the mass of the dry specimen [49].

$$WA\ (\%) = \frac{W - W_0}{W_0} \times 100 \quad (2)$$

here

W = the mass of the saturated surface dry surface specimen

W_0 = the mass of the dry specimen.

Upcoming studies will address the mechanisms of hydration and geopolymerization through systematic microstructural characterization, employing X-ray diffraction (XRD), scanning electron microscopy (SEM), and additional complementary analytical methods.

5- Results and discussion

The results of compressive strength tests at 28 and 90 days, along with rapid chloride penetration (RCPT), rapid chloride migration (RCMT), and water absorption at 90 days, are presented for the five mixture designs (M1–M5) under curing regimes A–E. All reported results represent the mean values of three specimens tested at each curing age. The measurements demonstrated satisfactory reproducibility, with the difference between maximum and minimum values within each set not exceeding 5%.

5-1- Compressive strength test results

Figs. 3 and 4 present the compressive strength values of the specimens at 28 and 90 days, respectively. Curing regime C was omitted up to 28 days due to its similarity with regime B. The results indicate that compressive strength increased with extended water curing. At 28 days, the highest strength was observed for mixture M2 under regime B, while at 90 days, mixture M4 under regime C exhibited the greatest strength.

Across all mixtures, regime B produced the highest compressive strength at 28 days, whereas regime D consistently yielded the lowest. At 90 days, regime C achieved the highest strength, with regime D remaining the lowest for all mixtures except M2. Steam curing (regimes D and E) did not significantly enhance compressive strength up to 90 days. Water curing improved performance due to continued slag hydration at later ages [50]. whereas steam curing negatively affected strength because of moisture loss through evaporation [51]. In this study, the incorporation of silica fume generally reduced 28-day compressive strength across most curing regimes.

5-1-1- M1 (100% OPC)

For the Portland cement specimen (M1), compressive strength under regimes D and E showed no significant difference compared to other curing regimes at 28 days. However, at 90 days, the strength of this specimen was lower in regimes D and E relative to the other curing conditions. Continuous water curing enhanced the compressive strength of M1 over time, reflecting the beneficial effect of prolonged hydration.

5-1-2- M2 (100% GGBS)

For the slag-based specimen (M2), curing in regime A resulted in reduced compressive strength at both 28 and 90 days compared to the control specimen. This reduction is attributed to the hydration process of Portland cement, which promotes faster strength development in the control mixture relative to slag-based concrete. In contrast, regimes B and C produced higher compressive strength in M2 than in the control specimen, with regime C yielding the maximum strength due to extended curing, which enhances the

geopolymerization mechanism and promotes long-term strength gain [52]. Curing in regimes A and B had limited influence on strength development beyond 90 days, reflecting the requirement of alkali-activated slag cement (AASC) for prolonged water curing. Under steam curing (regimes D and E), compressive strength values were lower than those obtained in regimes B and C but higher than those in regime A, indicating that steam curing provided a modest improvement despite the overall inferior performance compared to extended water curing.

5-1-3- M3 (92.5% GGBS + 7.5% SF)

Extended water curing for 90 days resulted in a notable increase in compressive strength, whereas curing for 7 and 28 days did not significantly enhance strength development. This behavior can be attributed to the reduction in early-age compressive strength, which is primarily linked to alterations in the Si/Al ratio within the reactive system. Variations in this ratio directly affect gel polymerization and microstructural evolution. The formation of binding phases in alkali-activated materials (AAMs) depends on the balanced dissolution and subsequent polycondensation of aluminosilicate species, leading to the generation of sodium aluminosilicate hydrate (N–A–S–H) or calcium aluminosilicate hydrate (C–A–S–H) gels [43, 53]. Excess silica introduced at early ages may delay aluminum incorporation into the gel framework, thereby slowing polycondensation and hindering early strength development [54, 55].

In addition, compared to the control specimens, the compressive strength of this mixture was lower under regimes A, B, D, and E, but higher under regime C. Regime A exhibited no significant influence on strength development, whereas regime B produced a 16% increase in compressive strength relative to the control.

5-1-4- M4 (85% GGBS + 15% LP)

Water curing proved highly effective for this specimen, with compressive strength increasing as curing duration was extended. The maximum strength, 72.2 MPa, was achieved at 90 days under regime C. In contrast, regime A showed little improvement, with values of 45.2 MPa at 28 days and 48 MPa at 90 days, indicating limited strength development due to the need for prolonged moisture availability to sustain polymerization. Supporting this observation, specimen M4 exhibited greater strength growth under regime B.

Specimens cured under regimes D and E demonstrated lower compressive strength compared to other regimes, with no significant improvement up to 90 days. Overall, compressive strength in regimes B and C exceeded that of the control specimens, whereas regimes A, D, and E produced lower values at 90 days.

5-1-5- M5 (75% GGBS + 7.5% SF + 17.5% LP*)*

Compressive strength increased with extended water curing, reaching its maximum in regime C at 90 days. In contrast, regime D consistently produced the lowest strength values among the curing conditions. Regimes D and E showed limited influence on strength development up to 90 days. A slight improvement in compressive strength was observed with elevated temperature compared to regime D at both 28 and 90 days.

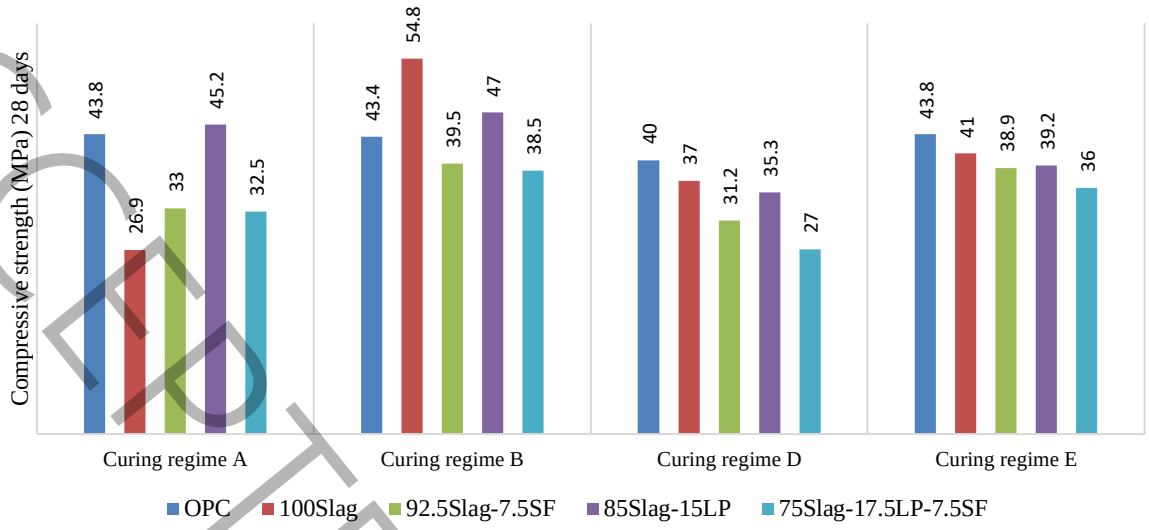

Fig. 3. 28-day compressive strength test results

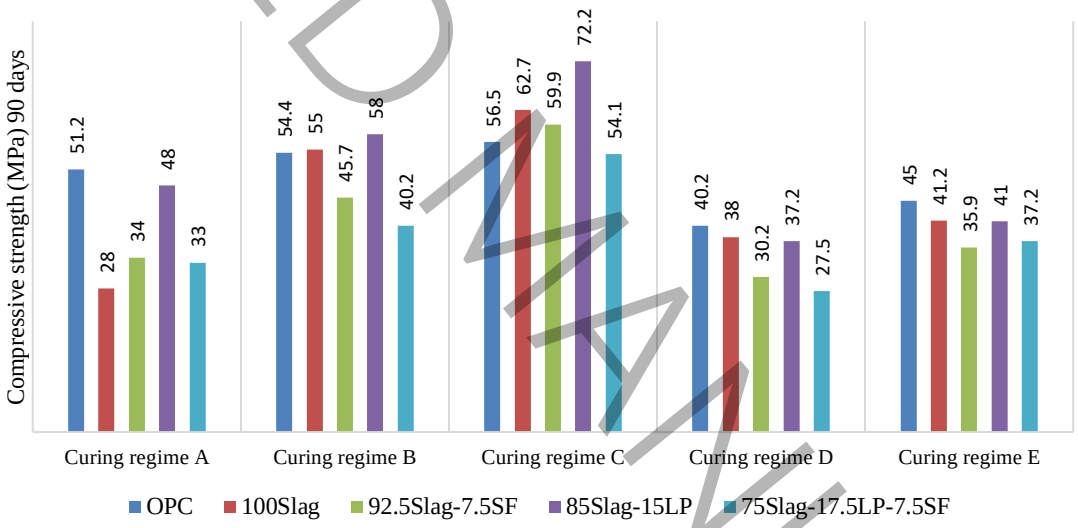

Fig. 4. 90-day compressive strength test results

5-2- Rapid chloride penetration test result

The results of the rapid chloride ion penetration test (RCPT) are presented in Fig. 5. Based on the classifications of ASTM C1202 and AASHTO TP 357-15 (Table 6), the lowest charge passed was consistently observed in regime C, while the highest values were recorded in regime D for specimens M1 and M3–M5, and in regime A for specimen M2. Specimen M4 exhibited lower charge passed values than the other mixtures across all curing regimes.

An increase in water curing duration led to a reduction in charge passed for all specimens, confirming the beneficial effect of extended curing. Furthermore, elevated temperature in regime E reduced the charge passed compared to regime D (40 °C), indicating improved resistance to chloride ion penetration under this condition.

5-2-1- M1 (100% OPC)

Chloride ion penetration for this specimen was classified as low under regimes A, B, and C, whereas regimes D and E exhibited moderate penetration. Extended water curing reduced the charge passed across all regimes, with the lowest value recorded in regime C.

5-2-2- M2 (100% GGBS)

Increasing the duration of water curing reduced the charge passed through the specimens, with the lowest values observed in regime C and the highest in regime A. Chloride ion penetration was classified as low in regimes B, C, D, and E, and moderate in regime A. The charge passed in regimes D and E was higher than in regimes B and C but lower than in regime A. Similarly, permeability in regime E was lower than in regimes A and D, yet higher than in regimes B and C.

The weak performance of specimens in regime A is attributed to insufficient water curing time, which hindered completion of the polymerization process. Compared to the control specimens, slag-containing mixtures exhibited higher charge passed in regime A, whereas in regimes B, C, D, and E, the charge passed was consistently lower than that of the control.

5-2-3- M3 (92.5% GGBS + 7.5% SF)

Increasing the duration of water curing reduced the charge passed through the specimen. Chloride ion permeability was classified as low in regimes B and C, and moderate in regimes A, D, and E. The highest charge passed was recorded in regime D (2510 C), while the lowest was observed in regime C. In regime E, the charge passed was lower than in regimes A and D but higher than in regimes B and C.

Compared to the control specimens, the charge passed was higher in regimes A, B, D, and E, whereas regime C exhibited lower values, confirming the beneficial effect of extended water curing.

5-2-4- M4 (85% GGBS + 15% LP)

For specimen M4, water curing resulted in lower charge passed values compared to thermal curing, with extended curing further reducing the charge passed. Chloride ion permeability was classified as low in regimes A, B, C, and E, and moderate in regime D. The highest charge passed was recorded in regime D, while the lowest was observed in regime C (1290 C). In regime E, permeability was greater than in regimes A, B, and C, but lower than in regime D.

Relative to the control specimens, M4 exhibited lower charge passed values in regimes A, B, C, and E, and nearly identical values in regime D.

5-2-5- M5 (75% GGBS + 7.5% SF + 17.5% LP)

With extended water curing, the charge passed through this specimen decreased. Chloride ion permeability was classified as moderate in regimes A, B, D, and E, and low in regime C. The highest charge passed was recorded in regime D (2650 C), while the lowest was observed in regime C (1710 C). Variations in regimes A and B were minimal, whereas increases were noted in the other regimes. In regime E, the charge passed was lower than in regimes A, B, and D but higher than in regime C.

Compared to the control specimens, this mixture design exhibited higher charge passed values in regimes A, B, D, and E, and lower values only in regime C.

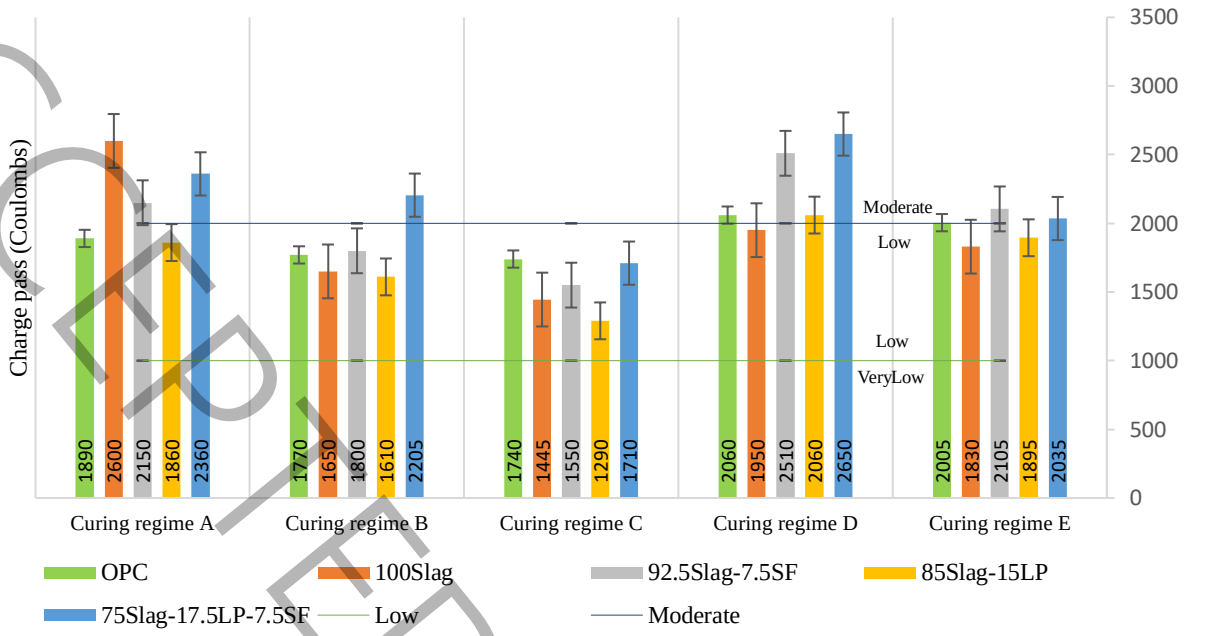

Fig. 5. 90-day charge passed (coulombs)

5-3- Rapid chloride migration test result

The results of the rapid chloride ion migration test (RCMT), presented in Fig. 6, indicate that the lowest chloride ion migration rate (CMR) was consistently obtained in regime C across all mixtures. The highest penetration rates were observed in regime D for specimens M3–M5, in regime E for specimen M1, and in regime A for specimen M2. Overall, specimen M4 exhibited lower CMR values compared to the other mixtures.

Extended water curing reduced the CMR in all specimens, confirming the beneficial effect of prolonged curing. Furthermore, elevated temperature (60 °C) in regime E produced a slight reduction in CMR compared to regime D.

5-3-1- M1 (100% OPC)

The chloride ion penetration rate of this specimen was lower under water curing compared to thermal curing, with extended curing up to 90 days further reducing the chloride migration rate (CMR). The lowest CMR was consistently obtained in regime C. In contrast, steam curing at 40 °C and 60 °C increased the CMR relative to water curing. According to the limits defined in Table 6, the chloride ion penetration rate of the control specimens remained within the low range across all curing regimes.

5-3-2- M2 (100% GGBS)

Increasing the duration of water curing reduced the chloride migration rate (CMR) in this specimen. The lowest CMR was obtained in regime C, while the highest was observed in regime A. Overall, the CMR remained within the low range across all curing regimes.

In regimes D and E, CMR values were higher than those in regimes B and C but lower than in regime A. Specifically, regime E produced lower values than regimes A and D, yet higher than regimes B and C. Regime D exhibited higher CMR than regimes B, C, and E, but lower than regime A.

The weak performance in regime A is attributed to insufficient water curing time, which disrupted the polymerization process and increased porosity, thereby elevating CMR. Compared with the control

specimens, this mixture showed higher CMR in regime A, while regimes B, C, D, and E consistently produced lower values than the control.

5-3-3- M3 (92.5% GGBS + 7.5% SF)

For specimen M3, increasing the duration of water curing reduced the chloride migration rate (CMR). Across all curing regimes, the CMR remained within the low range. The highest value was observed in regime D, while the lowest was obtained in regime C. In regime E, the CMR was lower than in regimes A and D but higher than in regimes B and C.

5-3-4- M4 (85% GGBS + 15% LP)

For specimen M4, water curing resulted in lower chloride migration rates (CMR) compared to thermal curing, with extended curing further reducing CMR. Values were classified as low in regimes A, B, D, and E, and very low in regime C. The highest CMR was observed in regime D, while the lowest was obtained in regime C.

In regime E, the CMR was higher than in regimes A, B, and C but lower than in regime D. Compared with the control specimens, M4 exhibited lower CMR in regimes A, B, and C, nearly equal values in regime E, and higher values in regime D.

5-3-5- M5 (75% GGBS + 7.5% SF + 17.5% LP)

Changes in CMR for specimens M5 decrease with increasing water curing time. Also, the CMR was classified as low across all curing regimes. The highest value was observed in regime D, while the lowest was obtained in regime C. In regime E, the CMR was lower than in regimes A, B, and D, but higher than in regime C.

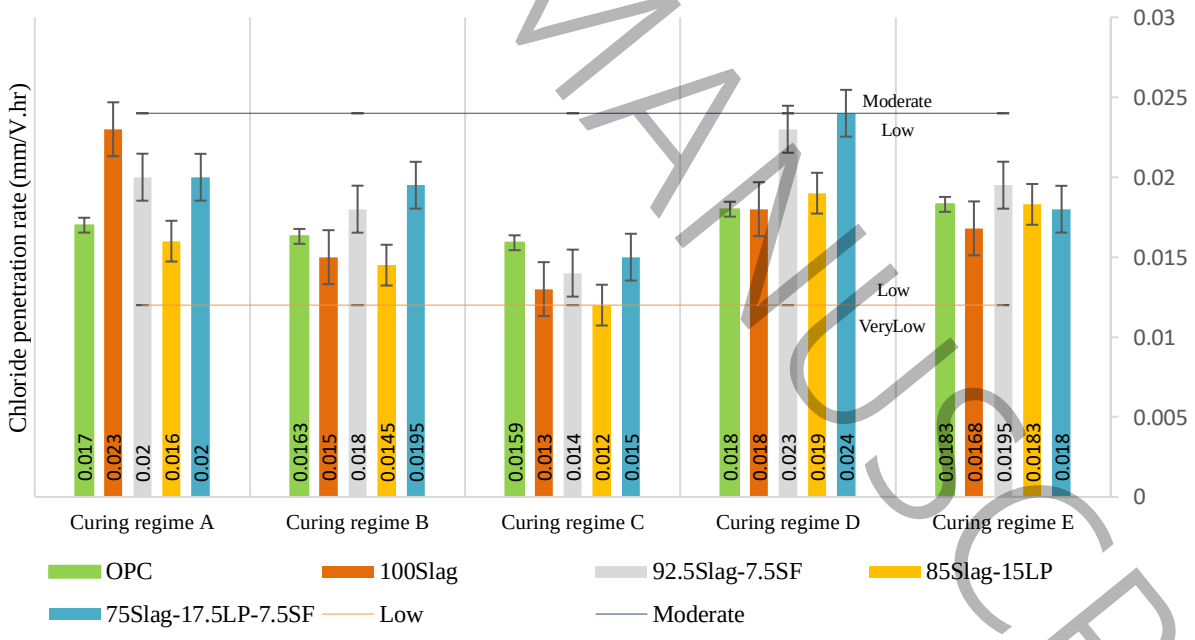

Fig. 6. 90-days chloride penetration rate (mm/V.hr)

5-4- Water absorption test result

The results of the volumetric water absorption test (Fig. 7) show that increasing the duration of water curing reduced the water absorption of all specimens. The lowest absorption was recorded for specimen

M5 in regime C, while the highest was observed for specimen M3 in regime A, excluding the control specimen. Specimen M4 exhibited the lowest absorption across all regimes except regime C.

Water absorption of specimens cured in water for 90 days (regime C) was lower than that of specimens cured under thermal conditions (regimes D and E). Furthermore, increasing the curing temperature from 40 °C to 60 °C produced a slight reduction in water absorption for specimens cured in regime E.

5-4-1- M1 (100% OPC)

By increasing the water curing time of specimen M1, the water absorption of this specimen decreased with extended water curing, with the lowest value obtained in regime C. In contrast, steam curing at 40 °C and 60 °C increased water absorption compared to water curing. Moreover, under thermal curing conditions, this specimen exhibited higher water absorption values than the other specimens cured at the same temperatures.

5-4-2- M2 (100% GGBS)

For specimen M2, increasing the duration of water curing reduced water absorption. The lowest absorption was obtained in regime C, while the highest was recorded in regime A. In regime E, water absorption was lower than in regimes A, B, and D, but higher than in regime C. The maximum absorption in regime A can be attributed to insufficient curing time in water (7 days), which limited hydration and densification of the matrix.

Compared with the control specimens, M2 exhibited lower water absorption in regimes D and E, but higher values in regimes A, B, and C.

5-4-3- M3 (92.5% GGBS + 7.5% SF)

The obtained results show a decrease in water absorption of specimen M3 with increasing duration of curing in water. Also, in regime A, the water absorption of this specimen reached 5.5%, representing the highest value among the curing regimes. The lowest absorption (3.85%) was obtained after 90 days of water curing in regime C. In regime E, water absorption was lower than in regimes A and D, equal to regime B, and higher than regime C. Compared with the control specimens, absorption was higher in regimes A, B, and C, but lower in regimes D and E.

5-4-4- M4 (85% GGBS + 15% LP)

The water absorption of specimen M4 also decreased with increasing duration of water curing. The highest absorption was recorded in regime A (3.7%), while the lowest was obtained in regime C (2.55%). In regime E, water absorption was lower than in regimes A, B, and D, but higher than in regime C. Compared with the control specimens, M4 exhibited lower water absorption across all curing regimes.

5-4-5- M5 (75% GGBS + 7.5% SF + 17.5% LP)

For specimen M5, water absorption decreased with increasing duration of water curing. The highest absorption was recorded in regime A (4.43%), while the lowest was obtained in regime C (2.4%). In regime E, absorption was lower than in regimes A, B, and D, but higher than in regime C. Compared with the control specimens, M5 exhibited lower absorption in regimes A, C, D, and E, but higher values in regime B. Furthermore, increasing the curing temperature from 40 °C to 60 °C in regime E produced a slight reduction in water absorption compared to regime D.

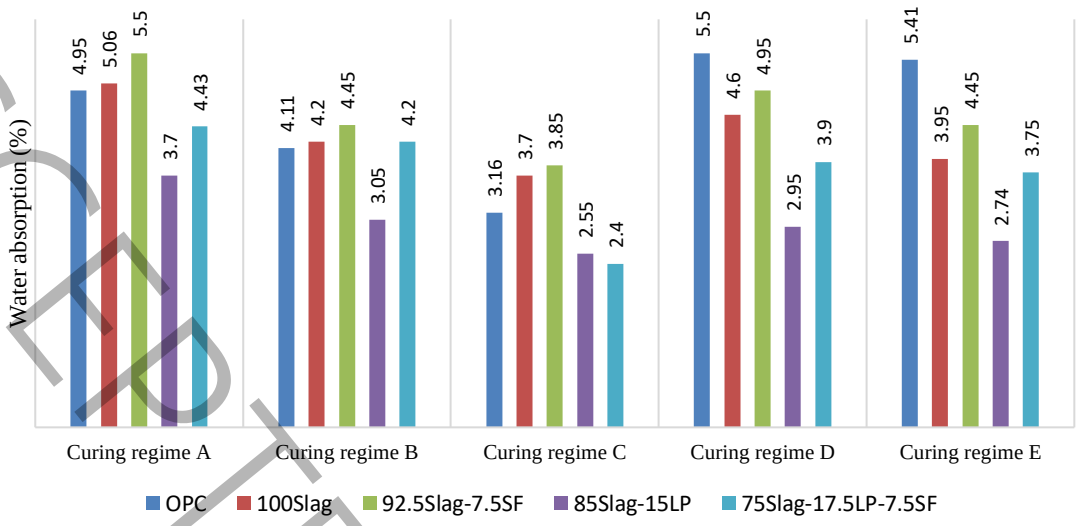

Fig. 7. 90-day volumetric water absorption test results (%)

5-5- Correlation between test results

To evaluate the correlation between the experimental results, the correlation coefficient was used to measure the strength and direction of association between variables. In addition, the coefficient of determination (R^2), ranging from 0 to 1, was employed to quantify the degree of correlation, with a value of 1.0 indicating perfect agreement. This statistical approach ensures the reliability of predictive models and diagrams [56].

According to the diagrams in Fig. 8, a significant correlation was observed between the compressive strength results at 28 and 90 days ($R^2 = 0.85$).

Strong correlations were also obtained between compressive strength and the results of the RCPT and RCMT tests ($R^2 = 0.92$). The pronounced correlation observed indicates that improvements in mechanical strength are inherently associated with reductions in ionic transport, reflecting the formation of a denser and more refined microstructure. This correlation suggests that fundamental microstructural features (namely enhanced gel connectivity and reduced pore continuity) concurrently govern both load-bearing capacity and resistance to chloride ingress. Thus, compressive strength may be considered not only a measure of mechanical performance but also a reliable indicator of durability in slag-based alkali-activated materials.

Furthermore, Fig. 9 shows that the strongest correlation was found between the chloride migration rate (CMR) and the charge passed ($R^2 = 0.96$), which allows conversion between these parameters with acceptable accuracy. In contrast, no meaningful correlation was identified between water absorption and the other test results. This lack of correlation can be attributed to the difference between internal absorption properties and the permeability characteristics of concrete.

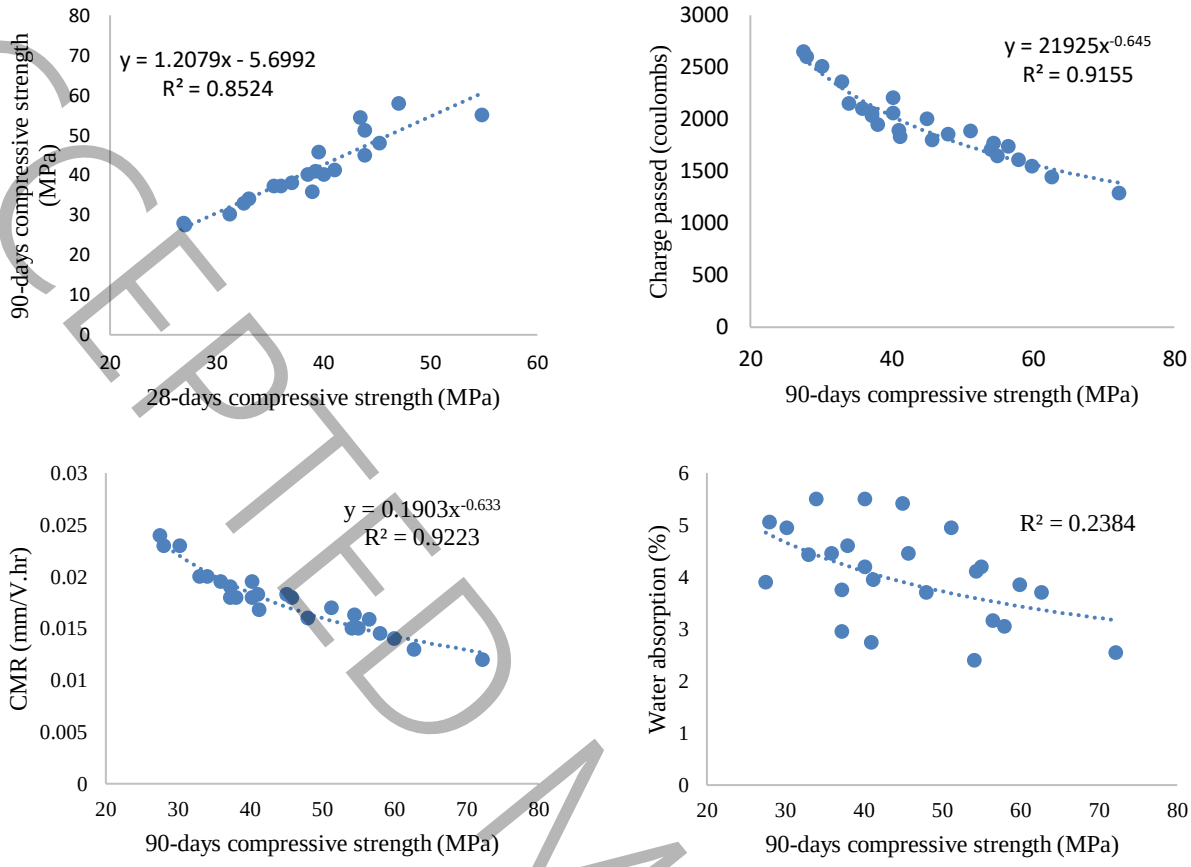

Fig. 8. Correlation between compressive strength and durability test results

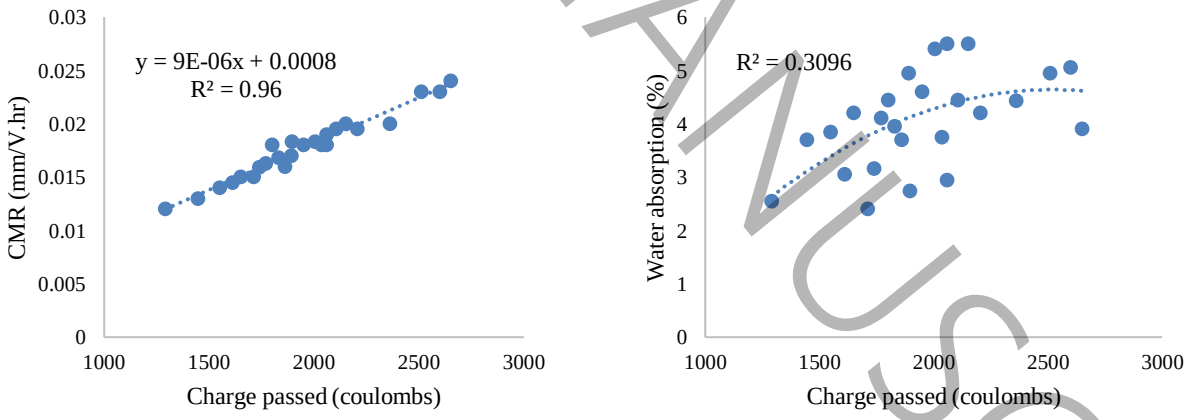

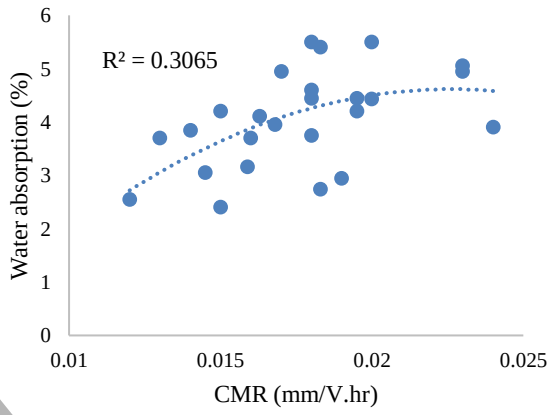

Fig. 9. Correlation between durability test results

Correlation curves obtained from laboratory measurements are case-specific, as they reflect the distinct experimental conditions and material under examination. Consequently, these Correlation should not be extrapolated beyond the scope of the particular study in which they were established.

5-6- Findings Summary

Compressive strength increased with extended water curing, with regime B producing the highest values at 28 days and regime C at 90 days. Regime D consistently yielded the lowest strength, and steam curing (regimes D and E) did not enhance performance.

Rapid chloride penetration (RCPT) results showed the lowest charge passed in regime C, while the highest values were observed in regime D (specimens M1, M3–M5) and regime A (M2). Specimen M4 consistently demonstrated superior resistance. Extended water curing reduced charge passage, and elevated temperature in regime E improved chloride resistance compared to regime D.

Rapid chloride migration (RCMT) results confirmed regime C as the most effective. Regime D produced the highest migration rates for M3–M5, regime E for M1, and regime A for M2. Specimen M4 exhibited the lowest migration values. Prolonged water curing reduced migration rates, while curing at 60 °C (regime E) slightly improved performance compared to regime D.

Volumetric water absorption decreased with longer water curing. The lowest absorption was recorded for M5 in regime C, while the highest was observed for M3 in regime A. Specimen M4 showed the lowest absorption across most regimes. Ninety-day water curing reduced absorption compared to thermal curing, and increasing curing temperature from 40 °C to 60 °C (regime E) slightly lowered absorption.

Mixture M4 (GGBS+LP) shows the best performance due to the dual role of limestone powder (LP). Physically, LP acts as a fine filler that densifies the binder matrix, refines pore structure, and accelerates product formation. Chemically, its calcium carbonate promotes the development and cross-linking of C–A–S–H gels in slag-based systems, resulting in enhanced strength and durability.

Compared to previous studies, none of the fabricated samples exhibited complete similarity with existing specimens, highlighting the innovative aspect of this research.

Correlation analysis revealed strong correlation between compressive strength at 28 and 90 days, and between compressive strength, RCPT, and RCMT. The strongest correlation was found between CMR and charge passed, and no significant correlation was observed between water absorption and other

durability indicators. The correlation equations and corresponding R^2 values are presented in Table 7, and it should be emphasized that these correlations are derived exclusively from the experimental data obtained in this study.

Table 7: Correlation between compressive strength and durability test results

Tests	Correlation between the test results	R^2
28-days and 90-days compressive strength	y = 1.2079x - 5.6992	R^2 = 0.8524
90-days compressive strength and Charge passed	y = 21925x - 0.645	R^2 = 0.9191
90-days compressive strength and CMR	y = 0.1903x - 0.633	R^2 = 0.9254
Charge passed and CMR	y = 9E-06x + 0.0008	R^2 = 0.96
90-days compressive strength and Water absorption	-	R^2 = 0.2257
Charge passed and Water absorption	-	R^2 = 0.3096
CMR and Water absorption	-	R^2 = 0.3065

6- Conclusion

This study examined the influence of five curing regimes (A–E), including water immersion and steam curing, on the compressive strength, water absorption, chloride ion penetration, and chloride ion migration of alkali-activated slag concrete incorporating different proportions of silica fume and limestone powder. The experimental findings are summarized as follows.

Compressive strength testing revealed that the specimen containing slag and limestone powder (M4) exhibited the highest performance, whereas the specimen incorporating slag, silica fume, and limestone powder (M5) showed the lowest. The most effective curing regime was water curing for 90 days, while steam curing for 24 hours at 40 °C produced the weakest results. Prolonged water curing consistently enhanced compressive strength across all specimens, and elevated curing temperature in regime E produced a slight improvement compared to regime D (40 °C) at both 28 and 90 days.

Rapid chloride ion penetration test (RCPT) results confirmed that M4 achieved superior performance under most curing regimes, while M5 consistently performed the weakest. The majority of specimens fell within the low to medium charge-passed range. Extended water curing reduced charge passage in all specimens, with the lowest values observed in regime C (90-day water curing). Furthermore, regime E demonstrated reduced charge passage compared to regime D (40 °C).

Rapid chloride migration test (RCMT) results indicated that the control specimen and M4 generally performed best across curing regimes, while no consistent weakest specimen could be identified. The highest chloride penetration rate was recorded for M5 under regime D (40 °C), whereas the lowest was observed for M4 under regime C (90-day water curing). Longer water curing durations reduced chloride penetration in all specimens, and regime E produced a slight decrease compared to regime D.

Volumetric water absorption testing showed that M5 achieved the best performance across all curing regimes. In contrast, M3 exhibited the weakest performance under water curing, while the control specimen (M1) performed worst under steam curing. Extended water curing reduced water absorption in all specimens, and regime E produced a slight decrease compared to regime D (40 °C).

Examining the correlation between the results of the conducted tests, a strong correlation between the results of 28 and 90 compressive strength tests and the results of the compressive strength test with RCPT

and RCMT has been obtained. In addition, a strong correlation between CMR and charge passed through the specimen has been obtained. Also, no proper correlation was found between the results of the water absorption test and the results of other tests. It should be emphasized that the correlations established in this study are specific to the experimental conditions and materials examined.

Finally, in line with the primary objective of this research (to develop geopolymer concrete suitable for conventional construction applications) it is recommended to employ a mixture comprising 85% slag and 15% limestone powder, cured in water under ambient temperature conditions.

References

[1] P K Mehta, P J Monteiro, Concrete microstructure, properties, and materials, McGraw-Hill Education, 2006.

[2] H Sujay, N A Nair, H S Rao, V Sairam, Experimental study on durability characteristics of composite fiber reinforced high-performance concrete incorporating nanosilica and ultra fine fly ash, Construction and Building Materials, 262 (2020) 120738.

[3] A Committee, ACI 201.2R - 16 Guide To Durable Concrete, American Concrete Institute, Farmington Hills, MI, 2016.

[4] Y Zhou, B Gencturk, K Willam, A Attar, Carbonation-induced and chloride-induced corrosion in reinforced concrete structures, Journal of Materials in Civil Engineering, 27(9) (2015) 04014245.

[5] L Bertolini, B Elsener, P Pedeferri, E Redaelli, R B Polder, Corrosion of steel in concrete: prevention, diagnosis, repair, John Wiley & Sons, 2013.

[6] P Mehta, P Monteiro, Concrete: Structure, Properties, and Materials, 2013.

[7] M S Shetty, A Jain, Concrete Technology (Theory and Practice), 8e, S. Chand Publishing, 2019.

[8] X Pardal, I Pochard, A Nonat, Experimental study of Si–Al substitution in calcium-silicate-hydrate (CSH) prepared under equilibrium conditions, Cement and Concrete Research, 39(8) (2009) 637-643.

[9] K L Scrivener, P Juilland, P J Monteiro, Advances in understanding hydration of Portland cement, Cement and Concrete Research, 78 (2015) 38-56.

[10] A Khodabakhshian, M Ghalehnovi, J De Brito, E A Shamsabadi, Durability performance of structural concrete containing silica fume and marble industry waste powder, Journal of cleaner production, 170 (2018) 42-60.

[11] R Taylor, I Richardson, R Brydson, Composition and microstructure of 20-year-old ordinary Portland cement–ground granulated blast-furnace slag blends containing 0 to 100% slag, Cement and Concrete Research, 40(7) (2010) 971-983.

[12] B Lothenbach, G Le Saout, E Gallucci, K Scrivener, Influence of limestone on the hydration of Portland cements, Cement and concrete research, 38(6) (2008) 848-860.

[13] E H Kadri, R Duval, Hydration heat kinetics of concrete with silica fume, Construction and Building Materials, 23(11) (2009) 3388-3392.

[14] M Adole, W Dzasu, A Umar, O Oraegbune, Effects of groundnut husk ash-blended cement on chemical resistance of concrete, ATBU Journal of Environmental Technology, 4(1) (2011) 23-32.

[15] P Murthi, V Sivakumar, Studies on acid resistance of ternary blended concrete, 2008.

[16] I S Oslakovic, R Roskovic, D Bjegovic, Concrete ability to resist chloride ions using ternary blended cement, Concrete Repair, Rehabilitation and Retrofitting II, CRC Press, 2008, 107-108.

[17] M A Aleem, P Arumairaj, Geopolymer concrete–a review, Int. J. Eng. Sci. Emerg. Technol, 1(2) (2012) 118-122.

[18] J Davidovits, Geopolymer chemistry and applications, Geopolymer Institute, Saint-Quentin, France, 2008.

[19] F Farooq, X Jin, M F Javed, A Akbar, M I Shah, F Aslam, R Alyousef, Geopolymer concrete as sustainable material: A state of the art review, Construction and Building Materials, 306 (2021) 124762.

[20] C K Ma, A Z Awang, W Omar, Structural and material performance of geopolymer concrete: A review, Construction and Building Materials, 186 (2018) 90-102.

[21] B B Jindal, Investigations on the properties of geopolymer mortar and concrete with mineral admixtures: A review, Construction and building materials, 227 (2019) 116644.
[22] B Singh, G Ishwarya, M Gupta, S Bhattacharyya, Geopolymer concrete: A review of some recent developments, Construction and building materials, 85 (2015) 78-90.
[23] G Qi, Q Zhang, Z Sun, Mechanical properties and hydration mechanism of super-sulfated cement prepared with ordinary Portland cement, carbide slag, and sodium silicate, Frontiers in Materials, 11 (2024) 1406045.
[24] X Xu, C Qi, X M Aretxabaleta, C Ma, D Spagnoli, H Manzano, The initial stages of cement hydration at the molecular level, Nature Communications, 15(1) (2024) 2731.
[25] E John, B Lothenbach, Cement hydration mechanisms through time–a review, Journal of Materials Science, 58(24) (2023) 9805-9833.
[26] P Duxson, A Fernández-Jiménez, J L Provis, G C Lukey, A Palomo, J S van Deventer, Geopolymer technology: the current state of the art, Journal of materials science, 42(9) (2007) 2917-2933.
[27] S A Bernal, J L Provis, Durability of alkali-activated materials: progress and perspectives, Journal of the American Ceramic Society, 97(4) (2014) 997-1008.
[28] H Z Jin, C X Qiu, Y S Li, B Liu, J Y Liu, Q Chen, X F Lu, C X Li, Q K Wang, Structural and functional design of geopolymer adsorbents: a review, Tungsten, 6(1) (2024) 48-76.
[29] A A Siyal, R M S R Mohamed, R Shamsuddin, M B Ridzuan, A comprehensive review of synthesis kinetics and formation mechanism of geopolymers, RSC advances, 14(1) (2024) 446-462.
[30] J L Provis, Geopolymers and other alkali activated materials: why, how, and what?, Materials and structures, 47(1) (2014) 11-25.
[31] V Athira, A Bahurudeen, M Saljas, K Jayachandran, Influence of different curing methods on mechanical and durability properties of alkali activated binders, Construction and Building Materials, 299 (2021) 123963.
[32] M Nodehi, T Ozbakkaloglu, A Gholampour, T Mohammed, X Shi, The effect of curing regimes on physico-mechanical, microstructural and durability properties of alkali-activated materials: A review, Construction and building materials, 321 (2022) 126335.
[33] M Saridemir, M Bulut, U Akca, Effects of different curing conditions on the long-term properties of alkali activated GBP plus GBFS mortars exposed to high temperatures, Construction and Building Materials, 321 (2022).
[34] V Jittin, P Madhuri, M Santhanam, A Bahurudeen, Influence of preconditioning and curing methods on the durability performance of alkali-activated binder composites, Construction and Building Materials, 311 (2021) 125346.
[35] A Runci, M Serdar, Effect of curing time on the chloride diffusion of alkali-activated slag, Case studies in construction materials, 16 (2022) e00927.
[36] A M Humad, J L Provis, A Cwirzen, Effects of curing conditions on shrinkage of alkali-activated high-MgO Swedish slag concrete, Frontiers in Materials, 6 (2019) 287.
[37] S Haruna, B S Mohammed, M Wahab, M Liew, Effect of paste aggregate ratio and curing methods on the performance of one-part alkali-activated concrete, Construction and Building Materials, 261 (2020) 120024.
[38] A Noushini, A Castel, The effect of heat-curing on transport properties of low-calcium fly ash-based geopolymer concrete, Construction and Building Materials, 112 (2016) 464-477.
[39] M Balcikanli, E Ozbay, Optimum design of alkali activated slag concretes for the low oxygen/chloride ion permeability and thermal conductivity, Composites Part B: Engineering, 91 (2016) 243-256.
[40] L Liu, M Xie, Y He, Y Li, A Wei, C Shi, Expansion behavior and microstructure change of alkali-activated slag grouting material in carbonate environment, Construction and building materials, 262 (2020) 120593.
[41] M Raghav, T Park, H M Yang, S Y Lee, S Karthick, H S Lee, Review of the effects of supplementary cementitious materials and chemical additives on the physical, mechanical and durability properties of hydraulic concrete, Materials, 14(23) (2021) 7270.

[42] J C M Arun K. Varshneya, Chapter 7 - Density and molar volume, Fundamentals of Inorganic Glasses (Third Edition), 2019, 173-186.
[43] M Boukendakdji, M Touahmia, B Achour, G Albaqawy, M Abdelhafez, K Elkhayat, E Noaime, The effects of steam-curing on the properties of concrete, Engineering, Technology & Applied Science Research, 11(2) (2021) 6974-6978.
[44] L Wang, W Wei, J Zhang, Y Hu, L Zhang, Effect of curing regime on the mechanical properties and durability of steam cured-concrete, Buildings, 13(7) (2023) 1697.
[45] H Yildirim, T Ilica, O Sengul, Effect of cement type on the resistance of concrete against chloride penetration, Construction and Building Materials, 25(3) (2011) 1282-1288.
[46] W Grace, Understanding AASHTO T277 and ASTM C1202 Rapid chloride permeability test, Technical Bulletin, 100 (2006).
[47] A S f Testing, Materials, ASTM C1202: Standard test method for electrical indication of concrete´ s ability to resist chloride ion penetration, ASTM West Conshohocken, 2022.
[48] T K Kim, S J Choi, J H Choi, J H J Kim, Prediction of chloride penetration depth rate and diffusion coefficient rate of concrete from curing condition variations due to climate change effect, International Journal of Concrete Structures and Materials, 13(1) (2019) 15.
[49] B EN, Testing concrete Method for determination of water absorption, 2020.
[50] S Aydın, B Baradan, Mechanical and microstructural properties of heat cured alkali-activated slag mortars, Materials & design, 35 (2012) 374-383.
[51] S F A Shah, B Chen, S Y Oderji, M A Haque, M R Ahmad, Improvement of early strength of fly ash-slag based one-part alkali activated mortar, Construction and Building Materials, 246 (2020) 118533.
[52] M F Nurruddin, H Sani, B S Mohammed, I Shaaban, Methods of curing geopolymer concrete: A review, International Journal of Advanced and Applied Sciences, 5(1) (2018) 31-36.
[53] J L Provis, Alkali-activated materials, Cement and concrete research, 114 (2018) 40-48.
[54] J y Liu, X t Deng, Q Ren, S Liu, Z b Ma, Influence of silica fume on drying shrinkage of alkali-activated carbon steel slag, Journal of Iron and Steel Research International, 31(12) (2024) 2953-2970.
[55] K Sothornchaiwit, W Dokduea, W Tangchirapat, S Keawsawasvong, C Thongchom, C Jaturapitakkul, Influences of silica fume on compressive strength and chemical resistances of high calcium fly ash-based alkali-activated mortar, Sustainability, 14(5) (2022) 2652.
[56] D Chicco, M J Warrens, G Jurman, The coefficient of determination R-squared is more informative than SMAPE, MAE, MAPE, MSE and RMSE in regression analysis evaluation, PeerJ Computer Science, 7(e623) (2021).